Partial Wetting in Trickle Bed Reactors:

Measurements Techniques and

Global Wetting Efficiency

Loïc BAUSSARON[1], *Carine JULCOUR-LEBIGUE*[1], *Anne-Marie WILHELM*[1],

Christophe BOYER[2], *Henri DELMAS*[1*]

1: Laboratoire de Génie Chimique de Toulouse (LGC), 5 rue Paulin Talabot BP 1301,

31106 Toulouse Cedex 1, France

2: Institut Français du Pétrole (IFP), IFP-Lyon, BP3, 69390 Vernaison, France

*corresponding author: Henri.Delmas@ensiacet.fr, tel: +33 (0)5 62 88 58 88, fax: +33 (0) 5 34 61 52 53

Abstract

Three very different techniques for measuring the catalyst wetted fraction -or wetting efficiency- in trickle bed reactors have been carried out and compared. The first one based on pressure drop data performed successively in single gas then liquid phase, then in gas-liquid phase is experimentally very simple but did not result in meaningful wetting efficiency estimation. The other ones, based on RTD analysis and on dye adsorption on wetted surfaces, gave similar results, and were used to investigate different parameters: liquid velocity and gas molecular weight and pressure by RTD, liquid-solid interaction or affinity (contact angle) and particle shape and diameter by dye fixation. The main operating parameter is the liquid velocity while the effect of gas flow is very weak. Higher solid-liquid affinity (heptane versus water) improves wetting efficiency only at very low liquid velocity ($<2\cdot10^{-3}$ m/s).

Keywords: trickle bed, wetting, tracer, pressure drop, contact angle

Introduction

Trickle bed reactors (TBR) are widely used in oil refinery and petrochemical industry, but also in fine chemistry, water treatment and electrochemical processes. Among multiphase reactors, TBR have probably the most complex hydrodynamics as trickling flow exhibits the unique feature of solid partial wetting under some conditions, mainly at low liquid flow rate. This phenomenon has been investigated for several decades but it is still badly predicted while for various reasons it has growing importance in oil industry. The main industrial applications of TBR concern catalytic fixed bed reactors implemented in oil refining for hydrotreatments such as hydrodesulfurization and hydrocracking. In the development and industrial operation of these reactors, partial wetting is a major issue due to three main reasons:

- The continuous drastic reduction of sulphur in benzene required by regulations for environment protection involves higher residence time, then lower liquid flow rate.

- Similarly heavier oils have to be more and more converted that requires longer residence time to reach the standards of purity.

- New catalysts and operating conditions are investigated in pilot scale reactors in order to improve catalysts efficiency and stability. These lab scale reactors are to be operated at the same liquid hourly space velocity as in commercial plants, then at very low liquid flow rate for small volume of catalyst tested. As the volume of catalyst tested has to be decreased for practical and economical reasons, partial wetting becomes a major issue for the correct operation of small size pilot plant.

This paper summarizes a part of a collaborative work between IFP Lyon and LGC Toulouse devoted to several aspects of partial wetting in trickle bed reactors. The complete work deals with wetting phenomena: effects of solid-liquid interaction i.e. wettability, effect of bed geometry and hydrodynamics, as well as with the convenient way to measure partial wetting at several scales: particle scale, bed cross section or whole bed. Here three measurement techniques are discussed and compared and a large amount of overall wetting efficiency data obtained by two validated techniques are reported and discussed.

Measurement techniques

Partial wetting in trickle bed reactors has been experimentally investigated by four main techniques: dynamic tracer technique[1-4], chemical reaction method[5,6], and more recently, hydrodynamic technique[7,8] and Magnetic Resonance Imaging technique, MRI[9]. Except MRI, all those approaches are overall, indirect and require a model of reactor involving hydrodynamic, transfer and/or kinetic parameters.

In this work three very different techniques have been used involving pressure drop measurement, residence time distribution of a tracer and dye adsorption. The last one is the most tedious as it needs to load the bed at each run and to perform image analysis but it is also the most informative as it gives

pattern of the liquid flow on each particle of a worked cross section. This technique is fully described by Baussaron[10] as well as local results on partial wetting at the particle level including axial and radial variations in the bed. The second technique based on tracer analysis involves a detailed model of tracer residence time distribution accounting for liquid axial dispersion, mass transfer at the catalyst boundary and non symmetrical diffusion in the catalyst pores due to partial wetting of the catalyst boundary. This complex modelling and the significance of tracer analysis depending on Péclet and Biot Numbers are described by Julcour-Lebigue et al.[11]. On the contrary, the first one using only pressure drop has been first proposed by Pironti et al.[7] and is experimentally extremely simple to implement. This technique and the tracer analysis technique have been performed in the same IFP equipment. The dye adsorption technique has been implemented at LGC Toulouse.

IFP pilot plant for pressure drop and tracer analysis

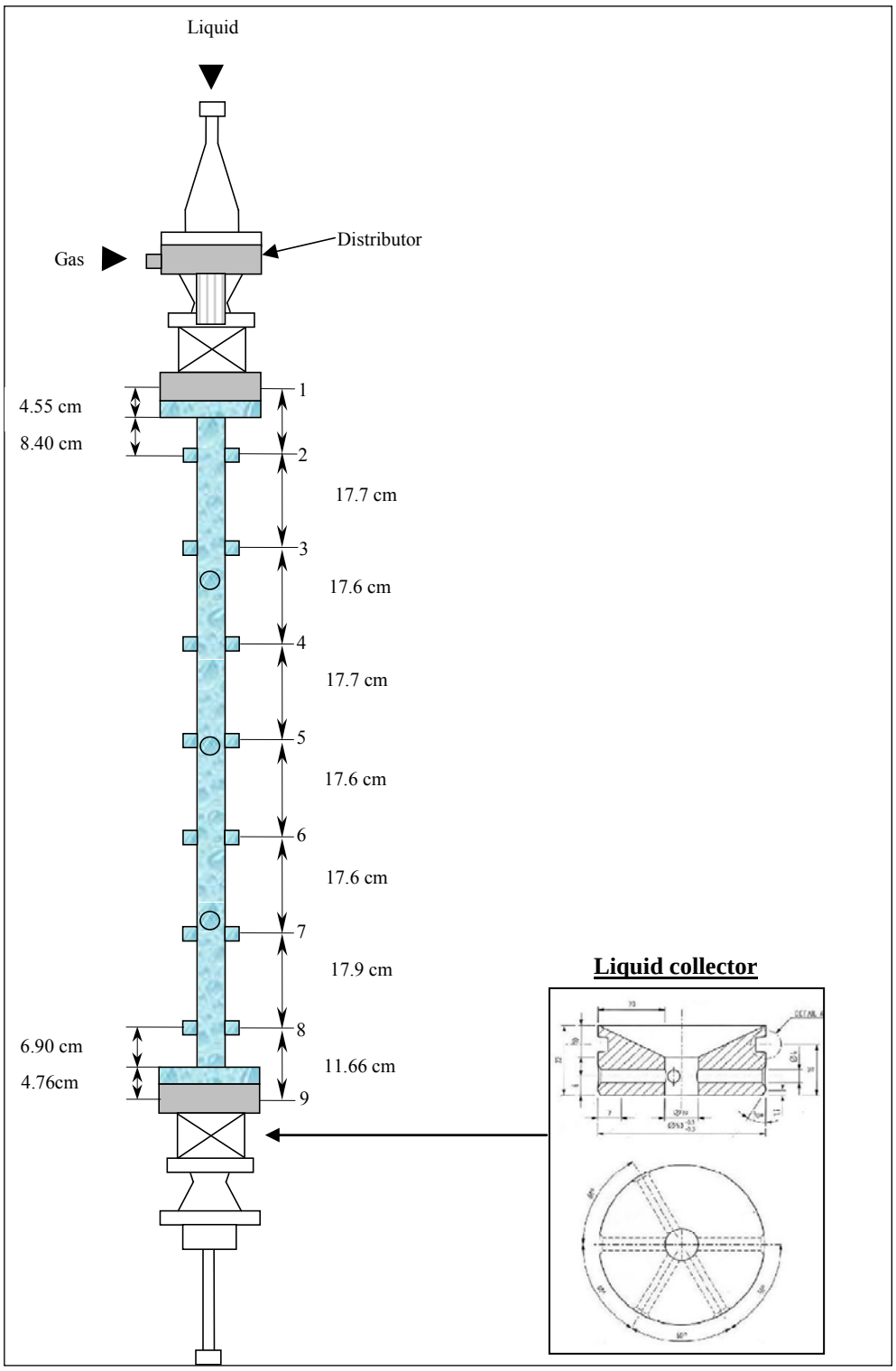

Figure 1. IFP pilot plant for pressure drop and tracer analysis.

The stainless steel reactor, 1.3 m long and 0.049 m internal diameter, is shown on Figure 1. It may be operated in single or two phase flow configuration up to 1 MPa and either up flow (flooded bed) or

down flow (trickle bed). A collector is placed at the bottom of the bed to avoid dead zones and to lead the liquid on the refractive index optical probe for continuous tracer concentration measurement at bed outlet. Pressure drop is measured by a Brooks differential pressure gauge. Liquid holdup may be obtained by two fast shut off valves and weighting of the trapped liquid after draining. Gas and liquid are separately introduced using a two phase distributor. Liquid and gas flow rates are measured by Coriolis flow meters.

Heptane is the liquid phase and isohexadecane is the liquid tracer. It is injected by using two four way (path) valves close to the reactor inlet. The injected volume is about 1.5% of the maximum liquid volume in the reactor. Refractive indexes of heptane and isohexadecane are 1.3847 and 1.4315, respectively, giving convenient tracer signals on the refractive index optical probes (Photonetics, see[12]) set both at the reactor top and bottom (two at each level to verify radial homogeneity of the tracer).

N_2 and SF_6, to simulate higher pressures, have been successively used as the gas phase. In the last case the liquid phase is previously saturated as SF_6 is highly soluble in heptane.

Porous particles are required for this tracer analysis based on the effect of partial wetting on tracer diffusion. Here alumina spheres are selected (pellets C, $d_p=2.5\cdot10^{-3}$ m, cf. table 1) as for the two other techniques.

Dye adsorption column

This column has been described elsewhere[10,13]. It has same diameter as the IFP pilot plant, similar gas and liquid distributor, and it is filled with particles following identical loading protocol.

Various types of alumina, with different structural densities ρ_S, internal porosities ε_p, specific areas a_S, sizes and shapes, have been used for these experiments. Their properties are detailed in Table 1.

The fixed bed can be operated at atmospheric pressure and ambient temperature only. The column consists in two concentric tubes, the inner one being divided into 11 slices. A piston is placed at its

bottom, so that the fixed bed can be pushed upwards and cut slice by slice to determine the axial evolution of the wetting efficiency.

	d_p [m]	ρ_S [kg/m^3]	ε_p [-]	a_S [m^2/g]	shape	ε_B [-]	supplier
Pellet A	$5.5\cdot10^{-3}$	2886	0.517	277	spherical	0.407	CALDIC (4-8 Grade D)
Pellet B	$2.5\cdot10^{-3}$	3804	0.75	192	spherical	0.397	SASOL (2,5/210_TKA809)
Pellet C	$2.5\cdot10^{-3}$	3195	0.591	83	spherical	0.372	IFP
Pellet D	$2.9\cdot10^{-3}$	3552	0.71	310	cylindrical	0.420	SASOL (z600200_TE142)

Table 1. Physical properties of the alumina particles.

Combined with image analysis, this technique provides detailed information on local partial wetting at several cross sections of the bed which can be integrated to get the volume averaged wetted fraction i.e. the wetting efficiency. The details of experiments and image analysis are reported in Baussaron[10] and Baussaron et al.[13]. Operating conditions are summarized in Table 2.

Studied parameters	Range
Liquid	Water, Heptane, Ethanol
V_{SL} [m.s^{-1}]	$(0.2\text{-}10)\cdot10^{-3}$
Gas	Nitrogen
V_{SG} [m.s^{-1}]	0-0.2
Catalyst pellet	Porous alumina
Shape	Sphere, Cylinder
d_p [m]	$(2.5\text{-}5.5)\cdot10^{-3}$
Pressure [MPa]	Atmospheric
Temperature [°C]	25

Table 2. Operating conditions in the dye-adsorption column.

Analysis of the significance of these techniques

Pressure drop

The original hydrodynamics method of determination of wetting efficiency from pressure drop and liquid holdup requires only very simple measurements: three pressure drops through the bed corresponding to gas flow, liquid flow and gas-liquid flow, the bed void fraction and the liquid holdup.

The principle of this method is based on a special definition of the wetting efficiency proposed by Pironti et al.[7].

$$f = \frac{(\tau_{LS} a_{LS})}{(\tau_{LS} a)} \text{ at same interstitial velocity } v_L^* \quad (1)$$

It is implicitly assumed that τ_{LS} the liquid-solid shear stress is the same in two phase flow and in liquid flow at same v_L^*.

Note that Kundu et al.[8] assumed same shear stress but at same superficial velocity.

The liquid-solid shear stress, $\tau_{LS,}$ is first determined in single phase liquid flow from the momentum balance, neglecting the friction force at the column wall.

$$\tau_{LS}.a = \frac{\varepsilon_B \Delta P_L}{L} + \rho_L g \varepsilon_B \quad (2)$$

$\tau_{LS}.a$ corresponds to the sum of the friction force on each particle per unit volume.

Correspondingly for the gas phase

$$\tau_{GS}.a = \frac{\varepsilon_B \Delta P_G}{L} + \rho_G g \varepsilon_B \quad (3)$$

For determining $\tau_{GS} a_{GS}$ and $\tau_{LS} a_{LS}$ in trickling flow, the momentum balances on the two phases are written as follows:

$$L.\tau_{GL}.a_{GL} + L.\tau_{GS}.a_{GS} = (\varepsilon_B - \varepsilon_L)\Delta P + (\varepsilon_B - \varepsilon_L)\rho_G g.L \quad (4)$$

$$L.\tau_{LS}.a_{LS} = \varepsilon_L \Delta P + \varepsilon_L \rho_L g.L + L.\tau_{GL}.a_{GL} \quad (5)$$

$$(1 - f) = \frac{(\tau_{GS}.a_{GS})}{(\tau_{GS}.a)} \text{ at same } v_G^* \quad (6)$$

From equations (1), (4), (5), (6) the wetting efficiency f, according to Pironti, is derived:

$$f_{Pironti} = \frac{-(\tau_{GS}.a) + \varepsilon_B \frac{\Delta P}{L} + g(\varepsilon_L \rho_L + (\varepsilon_B - \varepsilon_L)\rho_G)}{(\tau_{LS}.a) - (\tau_{GS}.a)} \quad (7)$$

It should be recalled that single phase shear stresses should be derived at same interstitial velocity using single phase pressure drop data which have been correlated according to Ergun equation:

$$\Delta P_F = L\left(A_F \frac{(1-\varepsilon_B)^2 V_{SF} \mu_F}{\varepsilon_B^3 d_p^2} + B_F \frac{(1-\varepsilon_B) V_{SF}^2 \rho_F}{\varepsilon_B^3 d_p} \right) \quad (8)$$

where, as shown on Figure 2, A_F and B_F coefficients are optimized for the two fluids (nitrogen and heptane) but do not differ much from the original Ergun values (A=150, B=1.8).

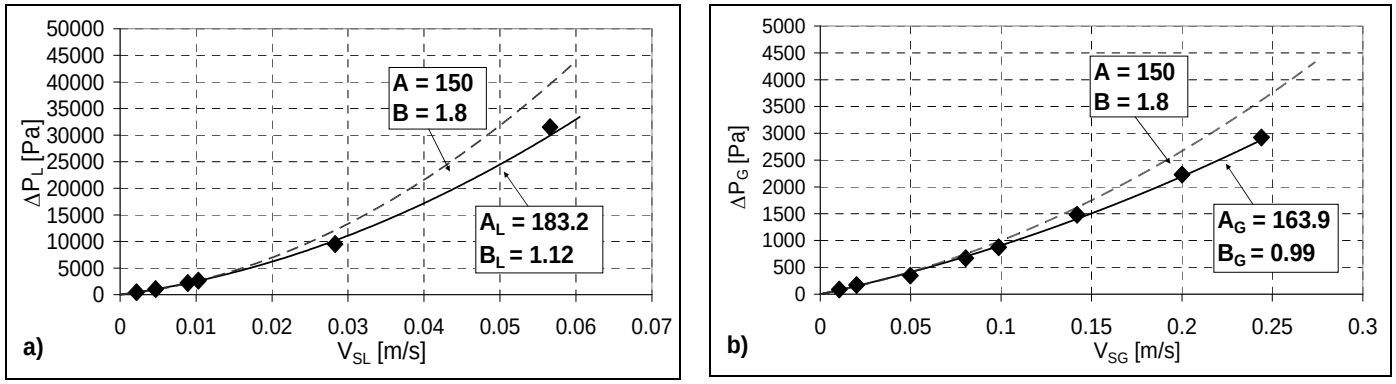

Figure 2. Pressure drop *vs.* superficial fluid velocity (pellets C): a) liquid, b) gas.

Figure 3 shows the variations of liquid holdup and pressure drop in trickle flow versus the liquid velocity at various gas flow conditions. Uncertainty on ΔP has been estimated at about 1%. The trends are usual with N_2, increasing gas velocity and density results in lower liquid holdup then higher shear stress and higher pressure drop. However unexpected results are shown for the heptane/SF_6 system as the liquid holdup increases with gas superficial velocity (3a), while the pressure drop strongly increases (3b). According to calculations using the correlation by Larachi et al.[14], a change in flow regime from trickling to pulsing flow might occur.

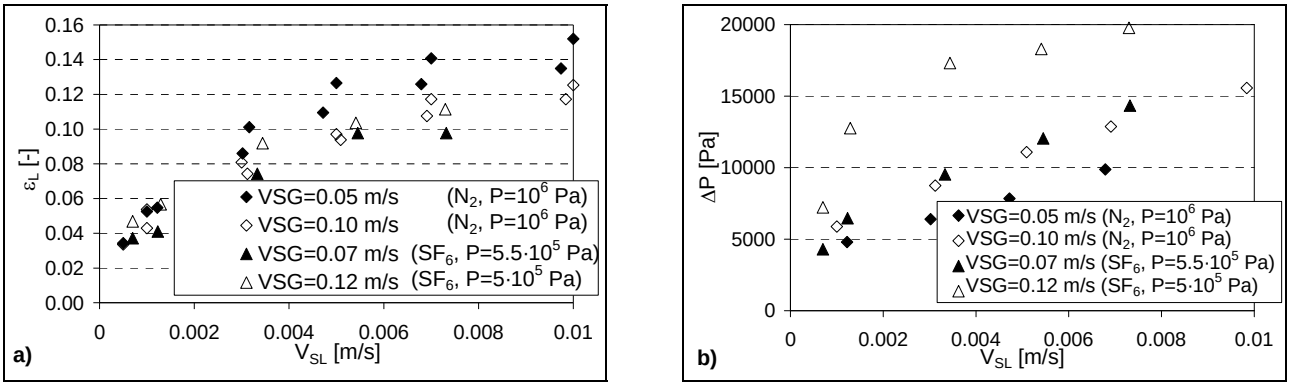

Figure 3. a) ε_L b) ΔP *vs.* V_{SL} (pellets C; heptane).

Using these data and equation (7) the wetting efficiency f has been derived. Results are plotted on Figure 4. The values of f are often much higher than 1 showing that this model is not convenient for quantitative measurement of the wetting efficiency, but trends observed have physical meaning: f increases at increasing liquid velocity and also at increasing gas velocity and density, which may be explained by a spreading effect of gas due to higher gas-liquid shear stress. Note that Pironti et al.[7] did not face these non physical data (f higher than 1) when working with water and air at atmospheric pressure. This suggests a wrong estimation of gas effect. As the fundamental hypothesis of equal shear stresses in single and two phase flow appears highly questionable, it has been decided not to use it and to come back to the true definition of $f = a_{LS}/a$.

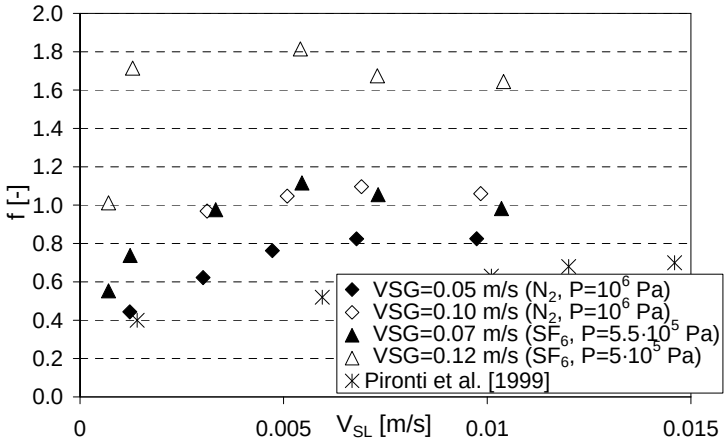

Figure 4. f (according to Pironti) *vs.* liquid velocity at various gas flow conditions (pellets C; heptane).

Momentum balances for the gas and liquid phases, equations (4) and (5), are still used. In these equations, τ_{LS} and τ_{GS}, the liquid-solid and gas-solid shear stresses, are to be modelled by closure equations. Let us consider a two phase flow in a vertical duct partly wetted. The liquid-solid friction force per liquid volume unit may be written as the sum of a laminar contribution and a turbulent one:

$$f_{LS} = \frac{j_L^{lam}\mu_L}{R_H^2} v_L^* + \frac{1}{2} j_L^{turb} \rho_L v_L^{*2} \frac{S_L}{V_L} \tag{9}$$

The hydrodynamic radius is the ratio of the flowing liquid volume to the wetted solid area

$$R_H = \frac{V_L}{S_L} \text{ where } \begin{cases} S_L = S_p f \\ V_L = V_R \varepsilon_L = \dfrac{V_p \varepsilon_L}{(1-\varepsilon_B)} \end{cases}$$

Finally in the case of a bed of spherical particles

$$R_H = \frac{V_L}{S_L} = \frac{V_p.\varepsilon_L}{(1-\varepsilon_B)f.S_p} = \frac{\varepsilon_L.d_p}{6(1-\varepsilon_B)f} \tag{10}$$

Using (9) and (10) and superficial liquid velocity $V_{SL} = v_L^* \varepsilon_L$ gives

$$f_{LS} = \frac{j_L^{lam}\mu_L (1-\varepsilon_B)^2 f^2}{\varepsilon_L^2} \frac{36}{d_p^2} \frac{V_{SL}}{\varepsilon_L} + \frac{1}{2} j_L^{turb} \rho_L \frac{6f(1-\varepsilon_B)}{\varepsilon_L d_p} \left(\frac{V_{SL}}{\varepsilon_L} \right)^2 \tag{11}$$

To account for tortuosity of the actual liquid flow through the bed the coefficients A_L and B_L of Ergun equation have been adjusted from single phase flow experimental data.

$$\begin{cases} j_L^{lam} \rightarrow A_L/36 \\ j_L^{turb} \rightarrow B_L/3 \end{cases}$$

The liquid-solid shear stress $\tau_{LS} = f_{LS} \frac{V_L}{S_L} = f_{LS} \frac{\varepsilon_L d_p}{6(1-\varepsilon_B)f}$ may then be expressed as:

$$\tau_{LS} = \frac{A_L}{6} \frac{\mu_L (1-\varepsilon_B) f}{\varepsilon_L^2 d_p} V_{SL} + \frac{B_L}{6} \rho_L \frac{1}{\varepsilon_L^2} V_{SL}^2 \tag{12}$$

Note that in equation (12) the first term of the shear stress involves f contrary to the implicit assumption in Pironti et al.[7] which could match only when the turbulent term is much higher than the laminar one and then at high liquid velocity and probably at complete wetting.

The same approach leads to the gas-solid shear stress,

$$\tau_{GS} = \frac{A_G}{6}\frac{\mu_G(1-\varepsilon_B)(1-f)}{{\varepsilon_G}^2.d_p}V_{SG} + \frac{B_G}{6}\rho_G\frac{1}{\varepsilon_G^2}V_{SG}^2 \qquad (13)$$

Attou et al.[15] and Iliuta and Larachi[16] proposed similar closure equations for the liquid-solid shear stress. Boyer and Ferschneider[17] verified it in the bubbling flow regime. Experimental pressure drop data obtained either in single phase flow or in two phase flow at sufficiently high liquid velocity for complete wetting to be expected (f=1 at $V_{SL}=10^{-2}$ m/s, cf. figure 7 for C type pellets) are used to determine experimental friction force f_{LS}^{mes} from

$$f_{LS}^{mes} = \left(-\frac{\Delta P}{L} + \beta_L\rho_L g + (1-\beta_L)\rho_G g\right).\left(\frac{1}{\beta_L}\right) \qquad (14)$$

and compared to predicted values from equation (11) on Figure 5 in single liquid flow (liquid full) or trickling flow at complete wetting.

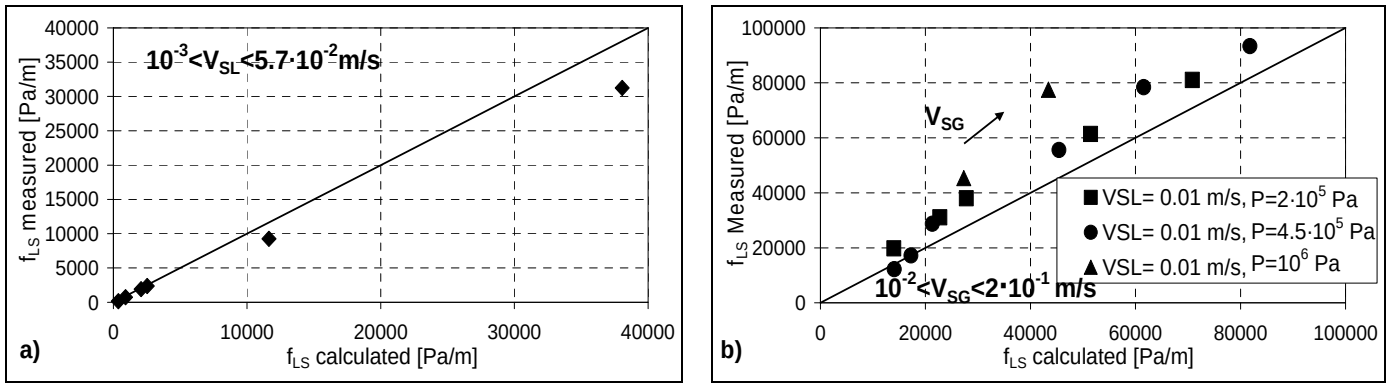

Figure 5. Comparison of measured and calculated f_{LS} (pellets C; heptane): a) liquid full, b) trickling flow.

In liquid full conditions the prediction is good, especially at low liquid velocities, while in trickle bed the effect of gas flow is clearly underestimated at high pressure and gas velocity. In order to improve

the estimation of the shear stress from pressure drop measurements and take into account the effect of gas flow momentum on liquid film tortuosity, an empirical correlation has been proposed and fitted on experimental data.

$$f_{LS} = \left[183.2 \frac{\mu_L (1-\varepsilon_B)^2 f^2}{\varepsilon_L^3 {d_p}^2} V_{SL} + 1.12 \rho_L \frac{(1-\varepsilon_B) f \rho_L}{\varepsilon_L^3 d_p} V_{SL}^2 \right] (1 + \Phi \rho_G V_{SG}^2) \qquad (15)$$

with the optimised value $\Phi = 2.48 \times 10^{-4}$ m.s^2.kg^{-1}.

This dependence on gas flow momentum refutes again Pironti assumption.

From this equation and the momentum balances (4) and (5) the equation giving f is derived

$$\begin{aligned} & -f^2.L.a\left[\alpha_G \frac{\mu_G V_{SG}}{(\varepsilon_B - \varepsilon_L)^2} + \alpha_L \frac{\mu_L V_{SL}}{{\varepsilon_L}^2} \Lambda \right] \\ & + f.L.a\left[2\alpha_G \frac{\mu_G V_{SG}}{(\varepsilon_B - \varepsilon_L)^2} + \frac{B_G}{6}\left(\frac{\rho_G {V_{SG}}^2}{(\varepsilon_B - \varepsilon_L)^2} \right) - \frac{B_L}{6}\left(\frac{\rho_L {V_{SL}}^2}{{\varepsilon_L}^2} \right) \Lambda \right] \\ & = L.a\left[\alpha_G \frac{\mu_G V_{SG}}{(\varepsilon_B - \varepsilon_L)^2} + \frac{B_G}{6}\left(\frac{\rho_G {V_{SG}}^2}{(\varepsilon_B - \varepsilon_L)^2} \right) \right] - \varepsilon_B \Delta P - gL((\varepsilon_B - \varepsilon_L)\rho_G + \varepsilon_L \rho_L) \end{aligned} \qquad (16)$$

where $\Lambda = (1 + \Phi \rho_G {V_{SG}}^2)$

and $\alpha_{fluid} = \frac{A_{fluid}}{6} \frac{(1-\varepsilon_B)}{d_p}$, $a_{GS} = (1-f).a$, $a_{LS} = f.a$, $a = \frac{6}{d_p}(1-\varepsilon_B)$

The wetted fraction f has been calculated according to equation (16) from the experimental pressure drops data already presented. Figure 6 shows these data and the corresponding correlation proposed by Iliuta and Larachi[16]. Here again trends are convenient but f is sometimes higher than 1 and probably always overestimated. It has been shown that f is very sensitive to the optimised parameters of closure law for liquid/solid friction force (equation (15)). Furthermore it was not possible to validate the closure law for gas/solid friction force since this would imply experiments in partial wetting conditions with values for wetting factor that should be accurately determined by another technique. The conclusion of this first part is then that convenient hydrodynamic measurement of the wetting efficiency is very difficult to achieve due to too high sensitivity to closure laws expression for gas/solid and liquid/solid

friction forces. Even with more mechanistic approach, theses closure laws are unable to model this complex two phase flow with a better accuracy than +/- 15 % in the best cases.

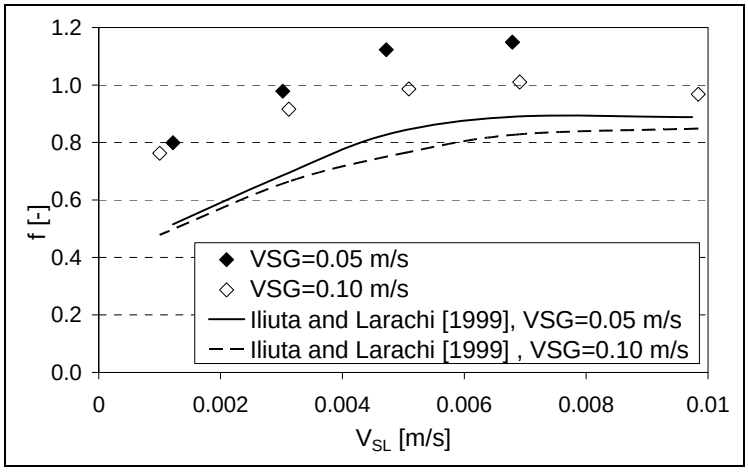

Figure 6. Estimation of f from (16) and comparison with Iliuta and Larachi[16] (pellets C; heptane ; N_2, $P=10^6$ Pa).

Tracer analysis

Although tracer technique is the most often used to determine wetting efficiency its fundamental basis have been clarified only recently[11]. Indeed the usual way to proceed was to perform tracer analysis in liquid full conditions (for example in up flow) and to optimise the effective diffusivity De in the catalyst pores. Finally an apparent diffusivity De_a was optimised from RTD experiment in trickle flow. The wetting efficiency f, i.e. the wetted fraction of the catalyst surface, was then calculated as either the ratio De_a/De or its square root. Unless a preliminary paper by Ramachandran et al.[18] this question was not discussed up to Julcour-Lebigue et al.[11].

The model developed by Julcour-Lebigue et al.[11] (later called "*2D model*") involving a complete resolution of the 2D diffusion in a spherical catalyst partly wetted was also extended to include the effects of axial dispersion, liquid-solid mass transfer, pattern of the wetted zone on a pellet, distribution of the wetting efficiency inside the bed and along the reactor length.

The model is based on the following assumptions:

- Complete pore filling (i.e. internal wetting) due to capillary forces.

- Spherical catalyst pellets.

- The outer surface of the pellet has a wetted zone around the north pole ($0 \leq \theta \leq \alpha$) and a dry zone underneath, so that:

$$f = (1 - \cos \alpha)/2 \qquad (17)$$

- The initial angle (α_i) of the wetted zone has also been varied to study the influence of the wetting pattern (polar or annular).

- No tracer transfer on dry zone.

- Same effective internal diffusivity in radial and angular directions.

- Negligible tracer vaporization.

- The adsorption equilibrium is instantaneous and linear.

- Liquid plug-flow with axial dispersion.

Model equations

Mass balance at the pellet scale:

$$\left(\varepsilon_p + \rho_S\left(1-\varepsilon_p\right)K\right)\frac{\partial C_i}{\partial t} = De\left(\frac{1}{r^2}\frac{\partial}{\partial r}\left(r^2\frac{\partial C_i}{\partial r}\right) + \frac{1}{r^2\sin\theta}\frac{\partial}{\partial\theta}\left(\sin\theta\frac{\partial C_i}{\partial\theta}\right)\right) \qquad (18)$$

with De, effective internal diffusivity of the tracer (m^2/s),

K, adsorption equilibrium constant of the tracer (m^3/kg),

ε_p, catalyst internal porosity,

ρ_S,"true" density of the solid (kg/m^3).

Boundary conditions:

$$r = 0 \qquad \forall\theta \qquad \lim_{r\to 0}\left(r^2\frac{\partial C_i}{\partial r}\right) = 0 \qquad (19)$$

(pellet center is neither a well nor a source of tracer)

$$\theta = 0, \pi \qquad \forall r \qquad \frac{\partial C_i}{\partial \theta} = 0 \qquad \text{(axisymmetry)} \tag{20}$$

$$r = r_p \qquad \begin{cases} -De\dfrac{\partial C_i}{\partial r} = k_S\left(C_i - C_L\right) & 0 \le \theta \le \alpha \\ \dfrac{\partial C_i}{\partial r} = 0 & \alpha \le \theta \le \pi \end{cases} \tag{21a,b}$$

(21a: liquid-solid flux from/to the wetted surface, 21b: no flux from/to the dry zone).

When the catalyst wetting is complete, equation (18) can be simplified into:

$$\left(\varepsilon_p + \rho_S\left(1-\varepsilon_p\right)K\right)\frac{\partial C_i}{\partial t} = De\left(\frac{1}{r^2}\frac{\partial}{\partial r}\left(r^2\frac{\partial C_i}{\partial r}\right)\right) \tag{22}$$

with boundary conditions:

$$r = 0 \qquad \lim_{r\to 0}\left(\frac{\partial C_i}{\partial r}\right) = 0 \qquad \text{(spherical symmetry)} \tag{23}$$

$$r = r_p \qquad -De\frac{\partial C_i}{\partial r} = k_S\left(C_i - C_L\right) \tag{24}$$

(which corresponds to the conventional model proposed by Colombo et al.[1] or "*1D (diffusion) model*")

Mass balance at the reactor scale:

$$\varepsilon_L\frac{\partial C_L}{\partial t} = -V_{SL}\frac{\partial C_L}{\partial z} + \varepsilon_L D_{ax}\frac{\partial^2 C_L}{\partial z^2} - \frac{\left(1-\varepsilon_B\right)}{V_p}\int_0^{\alpha} 2\pi r_p^2\, De\left.\frac{\partial C_i}{\partial r}\right|_{r=r_p}\sin\theta d\theta \tag{25}$$

with D_{ax}, liquid axial dispersion coefficient based on interstitial velocity (m^2/s),

ε_L, external liquid holdup,

V_{SL}, liquid superficial velocity (m/s).

Boundary conditions:

$$z=0 \qquad \varepsilon_L D_{ax}\left.\frac{\partial C_L}{\partial z}\right|_{z=0^+} = V_{SL}\left(C_L\big|_{z=0^+} - C_{inlet}\right) \tag{26}$$

$$z=L \qquad \left.\frac{\partial C_L}{\partial z}\right|_{z=L} = 0 \qquad (27)$$

A theoretical analysis of tracer concentration profiles at bed outlet in trickle-bed reactors was first performed, showing that tracer method may be used to accurately derive wetting efficiency in usual low axial dispersion conditions.

External mass transfer resistance, adsorption of the tracer, pattern of the wetted zone, and heterogeneity of wetting at the reactor scale were found to have only a slight effect on the outlet signal and the resulting wetting efficiency.

The main result is that in usual hydrodynamic and wetting conditions of trickle-beds (f >0.3), the wetting efficiency can accurately be evaluated from RTD data, using the simple *1D diffusion model* and the following formula:

$$f = (De_a/De)^{1/2} \qquad (28)$$

where De and De_a are the effective particle diffusivities optimised respectively in liquid-full conditions and in partial wetting regime (apparent effective diffusivity). The simple *1D diffusion model* assumes radial diffusion of species inside the particle with a spherical symmetry. This model can be deduced from model described above assuming a total wetting of the particle.

When using experimental RTD it was shown that optimisation of *1D model* from the complete experimental signals gives much more accurate results than using moments of RTD curves: less apparent effect of liquid velocity on the effective diffusivity in liquid full conditions, better liquid holdup estimation as compared with drainage measurements. It should be preferred to optimise simultaneously the liquid holdup and the apparent diffusivity, the first one validating the quality of the tracing experiment. Convenient trends and orders of magnitude were observed as will be shown later.

Here again the wetting efficiency derived from the complete *2D model* is very close to the one given by the *1D model* and equation (28) as shown on Figure 7. All next data will be treated with the simplified *1D model* and equation (28).

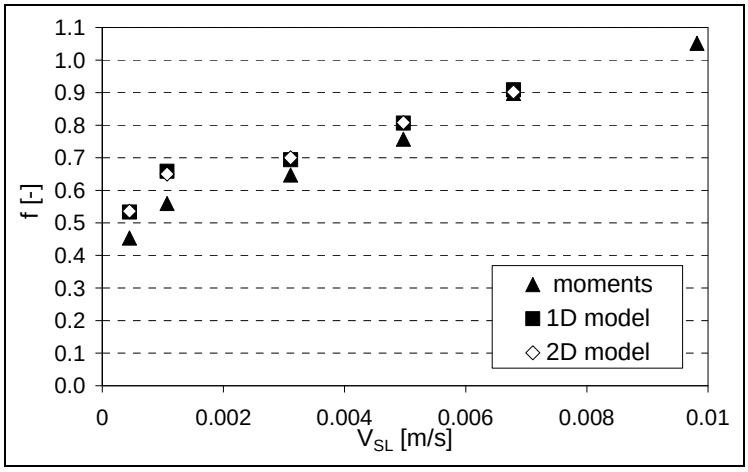

Figure 7. f *vs.* V_{SL} with various derivations (pellets C; heptane; N_2, $V_{SG}=5\cdot10^{-2}$ m/s, $P=10^6$ Pa).

Dye adsorption

As mentioned before this technique is very powerful as it provides the size and shape of the wetted zone on each half particle of a cross section (see Figure 8). A dye colorant is injected stepwise at column inlet and colorizes the particle external surface in contact with the liquid film. The experiment is performed within a delay preventing the migration of dye across the particles diameter. Images of solid particle in beds cross sections are processed to detect wetted surface and determine the wetting efficiency.

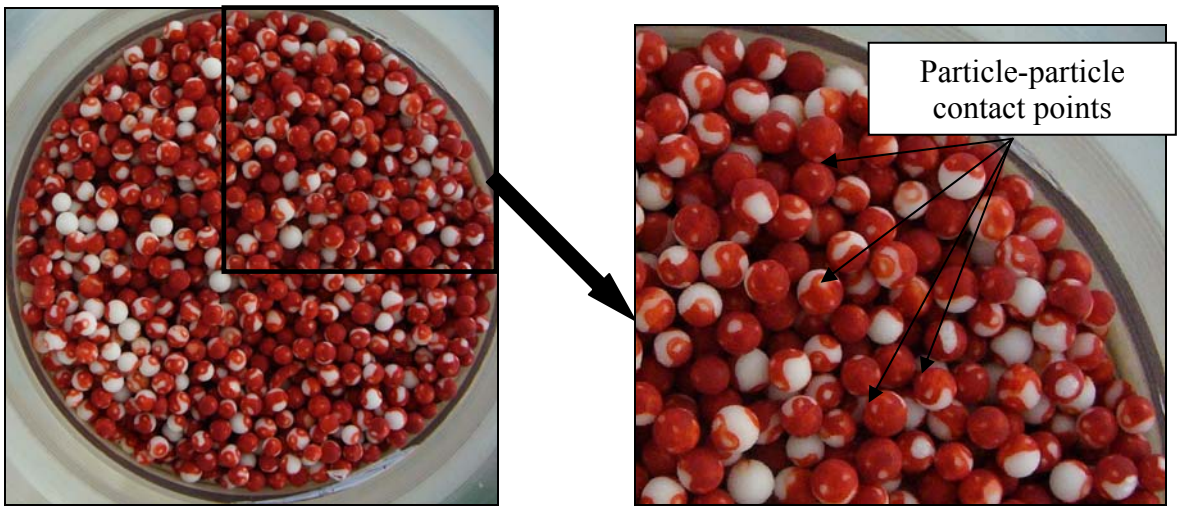

Figure 8. Sight of a cross section (pellets B: spherical alumina particles, $d_p=2.5\cdot10^{-3}$ m; heptane, $V_{SL}=6\cdot10^{-3}$ m/s; $V_{SG}=0$).

In addition particles from different slices of the bed were laid down and randomly set on plane plate, independently of their orientation in the bed, for a complementary image analysis. The data obtained by the two samples are in agreement within 10% as shown on Figure 9 at various axial locations. It should be noticed that the wetting efficiency does not vary axially as far as the bed has been pre-wetted.

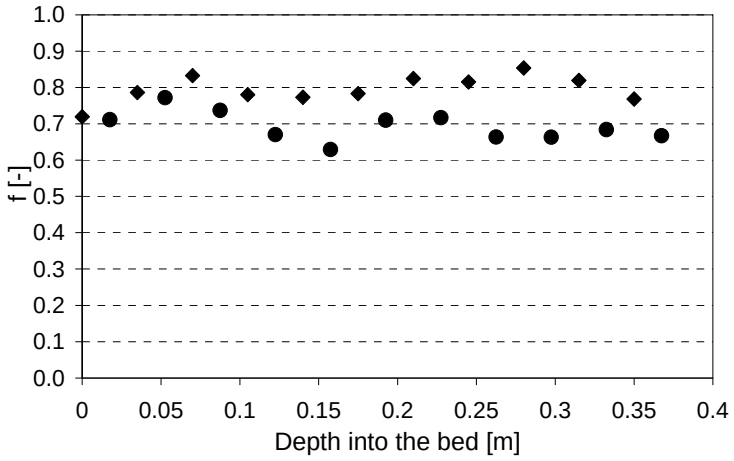

Figure 9. Comparison of wetting efficiency from cross section (◆) and from random analysis of laid down particles (●) at various depths into the bed (pellets B: spherical alumina pellets, $d_p=2.5\cdot10^{-3}$ m; heptane,$V_{SL}=6\cdot10^{-3}$ m/s; $V_{SG}=0$).

The main drawback is the need of rebuilding the bed for each experiment with fresh particles and some difficulty to get exactly the same void fraction despite a strict bed filling protocol.

All information concerning local analysis of partial wetting, axial and radial variations, effect of bed pre-wetting and of liquid distribution has been detailed elsewhere[10,13]. The main results are summarised as follows: partial wetting is axially and radially homogeneous after a few centimetres provided an efficient liquid distribution is performed at bed inlet. Wetting establishing length is longer with a single point liquid distribution and when the bed has not been prewetted. The present paper mainly deals with overall wetting efficiency on the whole bed and how it is controlled by several operating conditions, liquid velocity and also gas velocity, particle size and shape, liquid-solid wettability by testing different liquid/solid systems.

As for the tracer technique, the order of magnitude of the wetting efficiency and general trends are in agreement with literature. The comparison between tracer analysis and image analysis from dye adsorption is presented in Figure 10. Considering that dye adsorption and image analysis is a direct technique more reliable than tracer analysis which involves many complex transport phenomena of the tracer, it may be concluded that wetting efficiency is underestimated by 20 % maximum at very low liquid velocity.

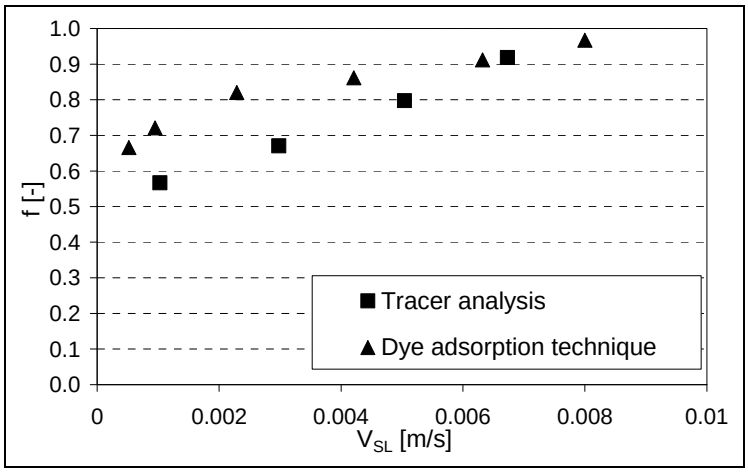

Figure 10. Comparison of wetting efficiency derived from tracer analysis and dye adsorption (pellets C; heptane; atmospheric pressure).

Results. Effect of operating parameters

Liquid velocity

Figure 11a shows the wetting efficiency as a function of superficial liquid velocity and a comparison with several correlations from literature. The distribution of this overall wetting efficiency on each particle is also presented on Figure 11b. When liquid velocity is decreased the main changes appear on

the extreme classes with clear reduction - from 42 to 6% - of the fraction of very wetted particles (0.9<f<1) and clear increase - from 5 to 22% - of nearly dry particles (0<f<0.1).

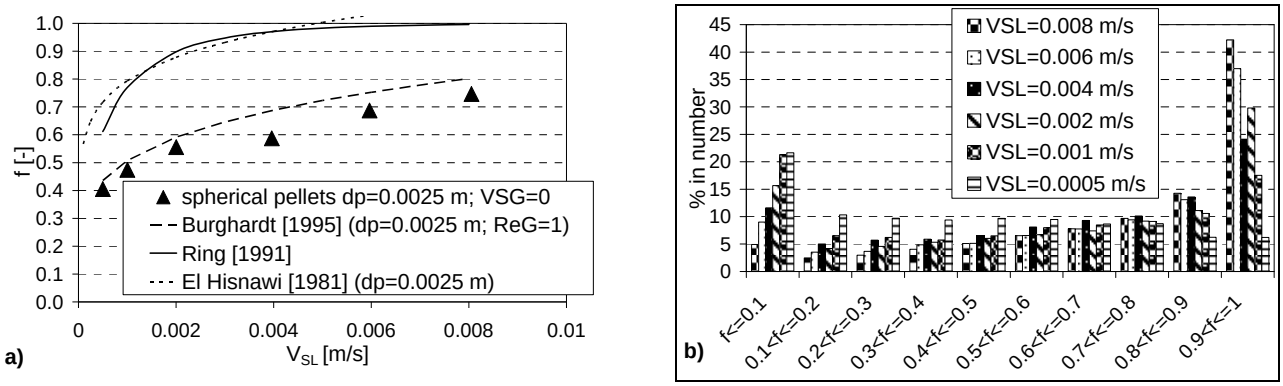

Figure 11. a) Overall wetting efficiency at various V_{SL}, b) Distribution of particle wetting efficiency (pellets B: spherical alumina particles, $d_p=2.5\cdot10^{-3}$ m; heptane; no gas velocity).

The correlation of Burghart et al.[3] gives better predictions of our experimental data than that of Ring and Missen[19] and El-Hisnawi et al.[20]. It should be noticed that Burghardt correlation cannot handle trickle flow condition without any gas flow, the comparison is then made using a low Reynolds number, $Re_G=1$.

Gas density and kinetic energy

According to literature different gas effects on wetting efficiency may be expected: either positive due to the liquid film spreading on the particle surface or negative due to the reduction of liquid holdup. In this work a very slight positive effect of increasing gas flow rate is observed, contrary to that predicted by Burghardt correlation as shown on Figure 12.

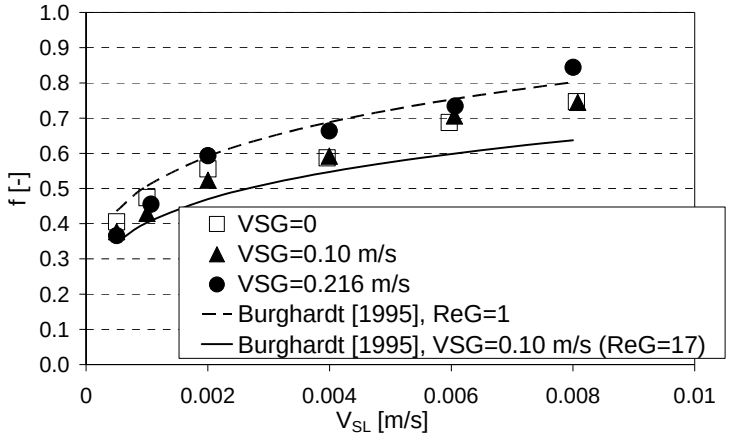

Figure 12. f *vs.* V_{SL} at different superficial gas velocities (pellets B: $d_p=2.5\cdot10^{-3}$ m; heptane; N_2, atmospheric pressure).

The effect of gas density - by varying either the gas molecular weight and/or the pressure - has been investigated by tracer analysis on IFP Pilot plant. The gas kinetic energy has been varied from 0.01 to 0.46 $kg.m^{-1}.s^{-2}$. Results are reported on Figure 13. No significant effect of the gas velocity or kinetic energy, as yet mentioned by dye adsorption measurements, was observed contrary to Al-Dahhan and Dudukovic[4].

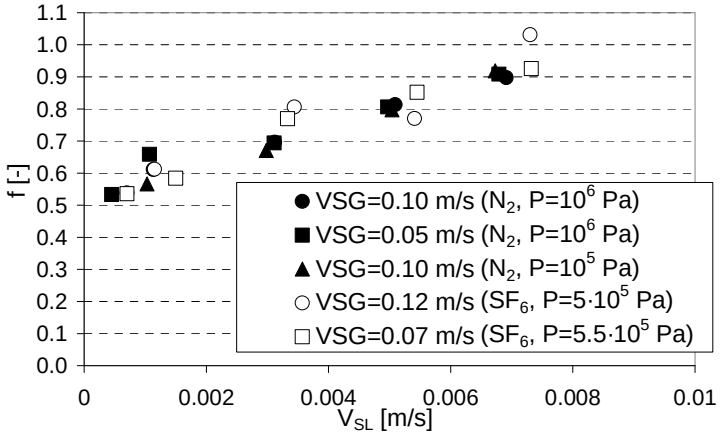

Figure 13. Effect of gas pressure and density on the wetting efficiency (pellets C; heptane).

Particle size and shape

Particle diameter

Two spherical particles of alumina of very similar affinity[10] and different diameter ($2.5 \cdot 10^{-3}$ m and $5.5 \cdot 10^{-3}$ m) have been used. Results at various liquid velocities are reported on Figure 14.

Wetting efficiency of large particles is reduced by about 12% at any liquid velocity. Nevertheless this result may also depend on the noticeable difference of bed porosity (0.407 for large particles and 0.372 for small particles). As increasing particle diameter and bed porosity are intuitively expected to have negative effect on the wetting efficiency, it was not possible to separate their effects since it is difficult to vary these parameters independently.

This effect of particle size is even slightly larger as predicted by Burghardt et al.[3], where bed porosity is not mentioned.

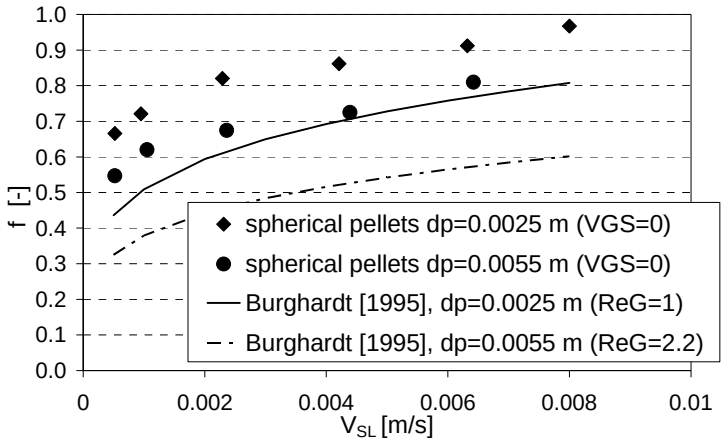

Figure 14. Effect of particle diameter on wetting efficiency (pellets C and A; heptane; atmospheric pressure).

Particle shape

Spherical particles are not much used in industrial trickle bed reactors where extrudated cylinders are often preferred. Worse liquid distribution is generally reported with cylinders. In this work wetting

efficiencies measured in similar conditions with spherical pellets (d_p=2.5·10^{-3} m) and cylinders (d_{pe}=2.9·10^{-3} m) of very similar wettability have been compared on Figure 15. In this case, cross section sights have been preferred as when laid down on plane plate cylinders never show their basis to the image analysis. As far as a dense packing of the bed is performed very similar wetting efficiencies are measured in usual liquid flow conditions (V_{SL}≥2·10^{-3} m/s). The shape of particles does not modify significantly the wetting efficiency.

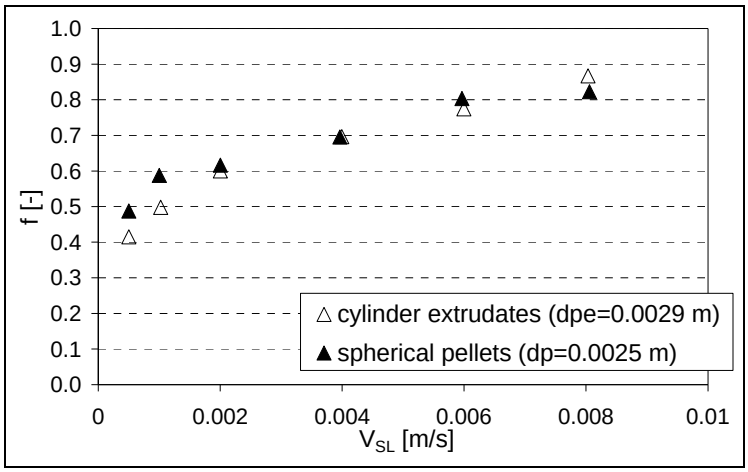

Figure 15. Effect of particle shape. Comparison of wetting efficiencies for spheres and cylinders (pellets D and B; heptane; atmospheric pressure).

Solid-liquid affinity

Three liquids, water, ethanol, heptane, have been successively used with the same alumina particles. For these liquids the contact angle have been determined according to Washburn technique, θ_c =65°, 39°, 0° (heptane as reference) respectively.

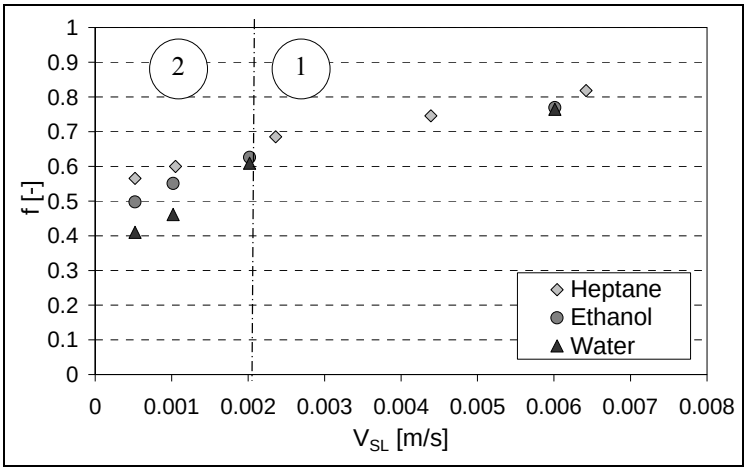

Figure 16. Effect of liquid-solid affinity on the wetting efficiency (pellets A: spherical alumina pellets, $d_p=5.5\cdot10^{-3}$ m; no gas velocity).

Data are reported on Figure 16 where two zones may be separated: at $V_{SL}<2\cdot10^{-3}$ m/s the wetted efficiency varies as expected, according to liquid solid affinity. On the contrary at higher liquid velocity hydrodynamics effects are much more important than interfacial effects and no difference is still observed with the 3 liquids. These results confirm that the hydrodynamics is the predominant phenomenon that controls wetting at liquid superficial velocity higher than $2\cdot10^{-3}$ m/s as assumed by authors up to now, but highlights that the intrinsic liquid/solid wettability controls wetting at very low liquid flow rate ($V_{SL} < 2\cdot10^{-3}$ m/s).

Conclusion

Partial wetting in trickle bed reactor has been experimentally investigated by means of three different techniques. The original hydrodynamic technique based on simple pressure drop measurements, using gas flow, liquid flow then gas-liquid flow, has been modified to improve the representation of shear

stresses. Nevertheless this method appeared unable to predict wetting efficiency with convenient accuracy in a wide range of operating conditions.

The second technique based on RTD measurements and convenient modelling including the combined effects of tracer axial dispersion, liquid-solid mass transfer at the catalyst surface and pore diffusion had previously been theoretically validated. This technique was implemented here in order to perform measurements at relevant pressure and gas velocity corresponding to hydrotreatments. It provided wetting efficiencies in good agreement with the data obtained by the third technique using direct image analysis of coloured wetted surfaces. As expected the main operating parameter is the liquid velocity. In addition the effect of gas velocity and density was found much smaller than predicted by previous correlations. A new parameter, the liquid-solid affinity, which was varied by changing the liquid phase has also been investigated in this work. It has no effect at moderate and high liquid velocity ($>2\cdot10^{-3}$ m/s) as implicitly assumed by correlations, but cannot be ignored at very low liquid flow rate where physicochemical interfacial effects overpass hydrodynamics.

Notations

A_F	Ergun coefficient, [-]
a	particle specific area, [m^{-1}]
a_{GL}	gaz-liquid interfacial area, [m^{-1}]
a_{LS}	liquid-solid interfacial area, [m^{-1}]
a_S	BET surface area, [m^2/g]
B_F	Ergun coefficient, [-]
C_i	normalized tracer concentration in the particle, [-]
C_L	normalized tracer concentration in the liquid bulk, [-]
D_{ax}	liquid axial dispersion coefficient, [m^2/s]
De	effective diffusivity, [m^2/s]

De_a	apparent effective diffusivity, [m^2/s]
d_p	particle diameter, [m]
d_{pe}	particle equivalent diameter, [m]
f	wetting efficiency, [-]
f_{LS}	friction force, [N/m^3]
j_L^{lam}	laminar coefficient in f_{LS} equation, [-]
j_L^{turb}	turbulent coefficient in f_{LS} equation, [-]
K	adsorption equilibrium constant of the tracer, [$m^3.kg^{-1}$]
k_S	liquid-solid mass transfer coefficient, [m/s]
L	reactor length, [m]
P	absolute pressure, [Pa]
R_H	hydraulic radius, [m]
r_p	particle radius, [m]
S_L	particle wetted area, [m^2]
S_p	particle area, [m^2]
t	time, [s]
V_{SG}	superficial gas velocity, [m/s]
V_{SL}	superficial liquid velocity, [m/s]
V_L	liquid volume, [m^3]
V_p	particle volume, [m^3]
V_R	reactor volume, [m^3]
v_G^*	interstitial gas velocity, [m/s]
v_L^*	interstitial liquid velocity, [m/s]
z	longitudinal coordinate, [m]

Greek Letters

α	angle defining the wetted polar zone, [°]
β_L	liquid saturation, [-]

ΔP	pressure drop, [Pa]
ε_B	bed porosity, [-]
ε_L	dynamic liquid retention, [-]
ε_p	particle porosity, [-]
θ	angle, [°]
θ_c	contact angle, [°]
μ_F	dynamic viscosity of fluid, [Pa.s]
ρ_F	fluid density, [$kg.m^{-3}$]
ρ_S	structural solid density, [$kg.m^{-3}$]
τ_{GS}	gas-solid shear stress, [Pa]
τ_{LS}	liquid-solid shear stress, [Pa]
Φ	parameter of hydrodynamic model, [$m.s^2.kg^{-1}$I]

Subscripts

G	Gas
GS	Gas-Solid interactions
L	Liquid
LG	Gas-Liquid interactions
LS	Liquid-Solid interactions
S	Solid

Literature cited

(1) Colombo, A. J.; Baldi, G.; Sicardi, S. Solid-liquid contacting effectiveness in trickle bed reactors. *Chem. Eng. Sci.* **1976**, *31 (12)*, 1101.

(2) Schwartz, J. G.; Weger, E.; Dudukovic, M. P. A new tracer method for determination of liquid-solid contacting efficiency. *AIChE J.* **1976**, *22 (5)*, 894.

(3) Burghardt, A.; Bartelmus, G.; Jaroszynski, M.; Kolodziej, A. Hydrodynamics and mass transfer in a three-phase fixed-bed reactor with cocurrent gas-liquid downflow. *Chem. Eng. Journal* **1995**, *58 (2)*, 83.

(4) Al-Dahhan, M. H.; Dudukovic, M. P. Catalyst wetting efficiency in trickle-bed reactors at high pressure. *Chem. Eng. Sci.* **1995**, *50 (15)*, 2377.

(5) Llano, J. J.; Rosal, R.; Sastre, H.; Diez, F.V. Determination of wetting efficiency in trickle-bed reactors by a reaction method. *Ind. Eng. Chem. Res.* **1997**, *36 (7)*, 2616.

(6) Ruecker, C. M.; Agkerman, A. Determination of Wetting Efficiencies for Trickle Bed Reactor at High Temperatures and Pressures *Ind. Eng. Chem. Res*. **1987**, *26 (1)*,164.

(7) Pironti, F.; Mizrahi, D.; Acosta, A.; Gonzalez-Mendizabal, D. Liquid-solid wetting factor in trickle bed reactors: its determination by a physical method. *Chem. Eng. Sci.* **1999**, *54 (17)*, 3793.

(8) Kundu, A.; Nigam, K. D. P.; Verma, R. P. Catalyst wetting characteristics in trickle bed reactors. *AIChE J.* **2003**, *49 (9)*, 2253.

(9) Gladden, L. F.; Mantle, M. D.; Sederman, A .J.; Yuen, E. H. L. Magnetic resonance imaging of single and two-phase flow in fixed-bed reactors. *Applied Magnetic Resonance* **2002**, *22*, 201.

(10) Baussaron L. Etude du mouillage partiel et du transfert de matière liquide-solide en réacteur à lit fixe arrosé. *Ph.D Thesis published at INP Toulouse*, **2005**: http://ethesis.inp-toulouse.fr/archive/00000249/01/baussaron.pdf

(11) Julcour-Lebigue, C.; Baussaron, L.; Delmas, H.; Wilhelm, A. M. Theoretical analysis of tracer method for the measurement of wetting efficiency. *Article in Press, Chem. Eng. Sci.* **2007**.

(12) Boyer, C.; Duquenne, A. M.; Wild, G. Measuring techniques in gas-liquid and gas-liquid-solid reactors. *Chem. Eng. Sci.* **2002**, *57 (16)*, 3185.

(13) Baussaron, L.; Julcour-Lebigue, C.; Wilhelm, A. M.; Boyer, C.; Delmas, H. Wetting Topology in Trickle Bed Reactors. *To be published in AIChE J.* **2007.**

(14) Larachi, F.; Laurent, A. ; Wild, G. ; Midoux, N. Effet de la pression sur la transition ruisselant-pulsé dans les réacteurs catalytiques à lit fixe arrosé. *Can. J. Chem. Eng.*, **1993**, *71 (2)*, 319.

(15) Attou, A.; Boyer, C.; Ferschneider, G. Modelling of the hydrodynamics of the cocurrent gas–liquid trickle flow through a trickle-bed reactor. *Chem. Eng. Sci.* **1999**, *54 (6)*, 785.

(16) Iliuta, I.; Larachi, F. The generalized slit model: Pressure gradient, liquid holdup and wetting efficiency in gas-liquid trickle flow. *Chem. Eng. Sci*. **1999**, *54 (21)*, 5039.

(17) Boyer, C.; Ferschneider, G. Experimental validation of a two-phase flow model for pressure drop and liquid hold-up in downflow packed bed bubble reactors. *Can. J. of Chem. Eng*. **2003**, *81 (3)*, 808.

(18) Ramachandran, P. A.; Dudukovic, M. P.; Mills, P. L. A new model for assessment of external liquid-solid contacting in trickle-bed reactors from tracer response measurements. *Chem. Eng. Sci.* **1986**, *41 (4)*, 855.

(19) Ring, Z. E.; Missen, R. W. Trickle-bed reactors: Tracer study of liquid holdup and wetting efficiency at high temperature and pressure. *Can. J. Chem. Eng.* **1991**, *69*, 1016.

(20) El-Hisnawi, A. A.; Dudukovic, M. P.; Mills, P. L. Trickle-bed reactors: dynamic tracer tests, reaction studies, and modeling of reactor performance. *ACS Symp. Ser.* **1982**, *196*, 421.

LIST OF CAPTIONS:

Figure 1. IFP pilot plant for pressure drop and tracer analysis.

Figure 2. Pressure drop *vs.* superficial fluid velocity (pellets C): a) liquid, b) gas.

Figure 3. a) ε_L b) ΔP *vs.* V_{SL} (pellets C; heptane).

Figure 4. f (according to Pironti) *vs.* liquid velocity at various gas flow conditions (pellets C; heptane).

Figure 5. Comparison of measured and calculated f_{LS} (pellets C; heptane): a) liquid full, b) trickling flow.

Figure 6. Estimation of f from (16) and comparison with Iliuta and Larachi[16] (pellets C; heptane; N_2, $P=10^6$ Pa).

Figure 7. f *vs.* V_{SL} with various derivations (pellets C; heptane; N_2, $V_{SG}=5\cdot10^{-2}$ m/s, $P=10^6$ Pa).

Figure 8. Sight of a cross section (pellets B: spherical alumina particles, $d_p=2.5\cdot10^{-3}$ m; heptane, $V_{SL}=6\cdot10^{-3}$ m/s; $V_{SG}=0$).

Figure 9. Comparison of wetting efficiency from cross section (◆) and from random analysis of laid down particles (●) at various depths into the bed (pellets B: spherical alumina pellets, $d_p=2.5\cdot10^{-3}$ m; heptane, $V_{SL}=6\cdot10^{-3}$ m/s; $V_{SG}=0$).

Figure 10. Comparison of wetting efficiency derived from tracer analysis and dye adsorption (pellets C; heptane; atmospheric pressure).

Figure 11. a) Overall wetting efficiency at various V_{SL}, b) Distribution of particle wetting efficiency (pellets B: spherical alumina particles, $d_p=2.5\cdot10^{-3}$ m; heptane; no gas velocity).

Figure 12. f *vs.* V_{SL} at different superficial gas velocities (pellets B: $d_p=2.5\cdot10^{-3}$ m; heptane; N_2, atmospheric pressure).

Figure 13. Effect of gas pressure and density on the wetting efficiency (pellets C; heptane).

Figure 14. Effect of particle diameter on wetting efficiency (pellets C and A; heptane; atmospheric pressure).

Figure 15. Effect of particle shape. Comparison of wetting efficiencies for spheres and cylinders (pellets D and B; heptane; atmospheric pressure).

Figure 16. Effect of liquid-solid affinity on the wetting efficiency (pellets A: spherical alumina pellets, $d_p=5.5\cdot10^{-3}$ m; no gas velocity).